From the New England Society for Vascular Surgery

Defining the radiation "scatter cloud" in the interventional suite

Omar P. Haqqani, MD, Prakhar K. Agarwal, BS, Neil M. Halin, DO, and **Mark D. Iafrati, MD,** *Boston, Mass*

Objective: **We hypothesized that fluoroscopic imaging creates radiation fields that are unevenly scattered throughout the endovascular suite. We sought to quantify the radiation dose spectrum at various locations during imaging procedures and to represent this in a clinically useful manner.**

Methods: **Digital subtraction imaging (Innova 4100; GE Healthcare, Waukesha, Wisc) of the abdomen and pelvis was performed on a cadaver in anteroposterior, left lateral, and right anterior oblique 45° projections. Radiation exposure was monitored in real time with DoseAware dosimeters (Phillips, Houston, Tex) in eight radial projections at distances of 2, 4, and 6 ft from the center of the imaged field, each at 5-ft heights from the floor. Three to five consecutive data points were collected for each location.**

Results: **At most positions around the angiographic table, radiation exposure decreased as the distance from the source emitter increased; however, the intensity of the exposure varied dramatically around the axis of imaging. With anteroposterior imaging, the radiation fields have symmetric dumbbell shapes, with maximal exposure perpendicular to the table at the level of the gantry. Peak levels at 4 and 6 ft from the source emitter were 2.4 times and 3.4 times higher, respectively, than predicted based on the inverse square law. Maximal radiation exposure was measured in the typical operator position 2 ft away and perpendicular to the table (4.99 mSv/h). When the gantry was rotated 45° and 90°, the radiation fields shifted, becoming more asymmetric, with increasing radiation doses to 10.9 and 69 mSv/h, respectively, on the side of the emitter. Minimal exposure is experienced along the axis of the table, decreasing with distance from the source (<0.77 mSv/h).**

Conclusions: **Quantifiable and reproducible radiation scatter is created during interventional procedures. Radiation doses vary widely around the perimeter of the angiography table and change according to imaging angles. These data are easily visualized using contour plots and scatter three-dimensional mesh plots. Rather than the concentric circles predicted by the inverse square law, these data more closely resemble a "scatter cloud." Knowledge of the actual exposure levels within the endovascular environment may help in mitigating these risks to health care providers. (J Vasc Surg 2013;58:1339-45.)**

Fluoroscopically guided vascular procedures are performed in large numbers in Europe and the United States, having increased annually during the past 20 years.[1] The benefits of endovascular procedures to patients are clear, but they also have the potential to produce high patient and occupational radiation doses that are a source of concern.[1-4] Although radiation exposure is a necessary risk of endovascular therapies, protection of our staff and patients requires a clear understanding of this exposure.

The increasing complexity of modern vascular interventions results in greater procedural difficulty and prolonged imaging that contributes to high radiation exposure to the endovascular team.[5,6] Some of the effects of prolonged radiation exposure include development of cataracts, cancer, and impaired fertility.[7]

Limiting the staff's exposure to large doses of radiation will reduce their risk of developing radiation-related illnesses, even though the risks cannot be eliminated entirely. In the general population of Switzerland, the overall annual radiation exposure from ambient and man-made sources is estimated to amount to about 4 mSv. Data obtained from experiments, clinical observations, and epidemiologic studies after intermediate to high radiation exposures attribute a mutagenic and carcinogenic potential at all radiation doses. The estimated additional probability that a fatal cancer will develop is 4×10^{-2}/Sv, and the probability of serious hereditary disorders within two generations is 1×10^{-2}/Sv.[8]

Varying procedural techniques, such as digital subtraction angiography (DSA), table height, magnification, collimation, imaging angle, and distance contribute to differences in radiation exposure.[9,10] The inverse square law states that radiation levels decrease in proportion to the square of the distance from the source emitter in a vacuum.[11-13] Although this physical reality is not disputed, the endovascular suite is certainly not a vacuum. The many variations of room configurations and imaging techniques, as well as patient characteristics, create multiple relevant variables that might influence scatter radiation levels.

Unfortunately, there are no existing models that define real-life scatter radiation dynamics. Modern vascular

From the Department of Vascular Surgery, The Cardiovascular Center, Tufts Medical Center.

Supported by the Society of Vascular Surgery Clinical Research Seed Grant.
Author conflict of interest: none.
Presented at the Thirty-eighth Annual Meeting of the New England Society for Vascular Surgery, Providence, RI, September 16-18, 2011.
Additional material for this article may be found online at www.jvascsurg.org.

Reprint requests: Omar P. Haqqani, MD, Department of Vascular Surgery, Mid Michigan Medical Offices, 4011 Orchard Dr, Ste 4006, Midland, MI 48640 (e-mail: omar.haqqani@midmichigan.org).

The editors and reviewers of this article have no relevant financial relationships to disclose per the JVS policy that requires reviewers to decline review of any manuscript for which they may have a conflict of interest.
0741-5214/$36.00

http://dx.doi.org/10.1016/j.jvs.2013.01.025

imaging requires methodologies that ensure excellent fidelity and ease of use while minimizing the risk of harm to the patient and the medical team. Assessment of this risk requires a quantitative real-time measure of exposure that can be used to determine methods to reduce exposure.

The goal of this study was to look at actual radiation levels and determine effects of scatter radiation in a typical interventional suite, under various fluoroscopic imaging conditions. We hypothesized that the inverse square law might not accurately predict the intensity of radiation exposure experienced around the angiography table and therefore might result in suboptimal choices regarding imaging techniques and staff positioning during procedures. The conditions examined include standard anteroposterior (AP) and left lateral and right anterior oblique (RAO) 45° projections.

METHODS

Various clinical imaging conditions typical in interventional procedures were simulated using a recently deceased nonformaldehyde-fixed male cadaver with a body mass index of 27 kg/m^2 and with no implanted prosthetic devices. The cadaver was imaged with a fixed C-arm Innova 4100 angiographic system (GE Healthcare, Waukesha, Wisc) equipped with a 40-cm solid-state detector. All scatter radiation levels were measured during digital subtraction angiography (DSA) imaging under automatic exposure control. The generator technique was set at "Adult Abdomen Aorta." This technique uses a base of 0.1 mm/Cu and 85-kV tube voltage when set to the low detail level and 0 mm/Cu on normal detail. Technique and filtration vary dynamically based on manufacturer's dose curve trajectories.

The baseline image to which all comparisons were made is an abdominal/pelvic angiogram. This index image was an AP projection: distance from the floor to the table top (table height), 90 cm; source to image-receptor distance, 52 cm; fully open horizontal and vertical collimation; detector height, 10 cm above the cadaver exit surface; 40-cm field of view, radiation field centered over the pelvis region, automatic exposure control with 85-kVp tube voltage, and 4 frames/s with 0 magnification.

Scatter radiation energy was recorded with DoseAware badges (Phillips, Houston, Tex) positioned at 5 ft above the floor in eight radial projections at 2, 4, and 6 ft from the center of the imaged field. The radial projections were defined at 45° intervals from the source detector (range, 0°-315°; Fig 1). DSA imaging was performed with pulsed fluoroscopy at 30 pulses/s for a total of 10 seconds. The DoseAware system measures the instantaneous radiation exposure at each badge and records these data in 1-second increments. A brief ramp up and decline is noted with each imaging cycle; therefore, we captured three to five consecutive data points within the plateau section for each experimental cycle. In this experiment, we varied a single angiographic parameter while maintaining all other imaging variables constant, recording radiation doses at multiple locations around the angiography table. No radiation shielding was used. Isodose curves were generated using interpolation from the measured data points.

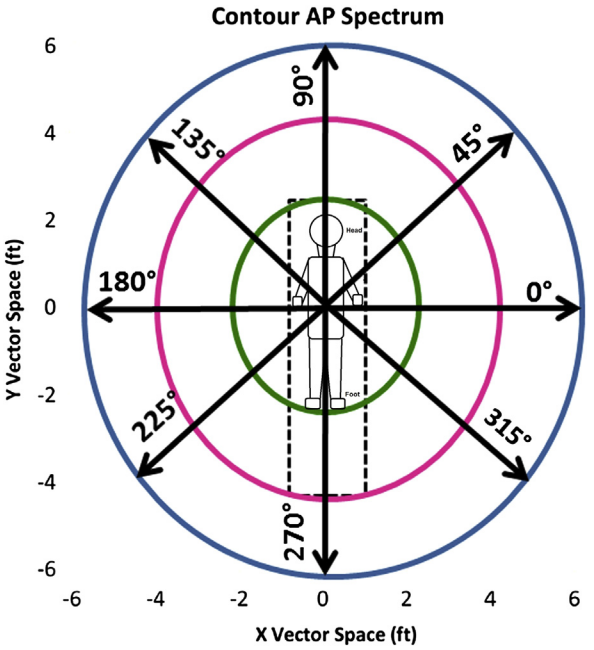

Fig 1. Schema for radiation scatter badge detector positions at 2 ft (*green*), 4 ft (*pink*), and 6 ft (*blue*) distances from the center position. Radial projections were defined at 45° intervals from the source detector (range, 0°-315°). The patient's head is at 90°. *AP,* Anteroposterior.

Data analysis. Data were collected from the DoseAware dosimeter badges and extracted using the DoseManager software (Philips). Custom macroprogramming was created to time-stamp imaging maneuvers and synchronize them with measured dosage readings. Three to five data points reflecting the plateau segment were collected for each varying angiographic parameter. The data were entered and analyzed in GraphPad Prism 5 software (GraphPad Inc, La Jolla, Calif). Data points were analyzed for statistical significance with sum-of-squares *F*-test.

Linear isodose plots were interpolated for distances of 2, 4, and 6 ft for each radial projection. Radial projections were plotted on contour and three-dimensional mesh plots with SigmaPlot 12 software (Systat Software Inc, Chicago, Ill) for each respective projection.

RESULTS

AP imaging. Digital subtraction AP imaging yields a bimodal scatter distribution pattern (Fig 2). Maximal exposure to radiation occurs along the lateral edges of the angiographic table at the 2-ft distance perpendicular to the dose emitter (4.53-4.98 mSv/h; Fig 3). The radiation exposure at the ends of the table (head-foot axis) is <0.77 mSv/h.

Left lateral projection imaging (full lateral). Digital subtraction imaging in the left lateral projection yields

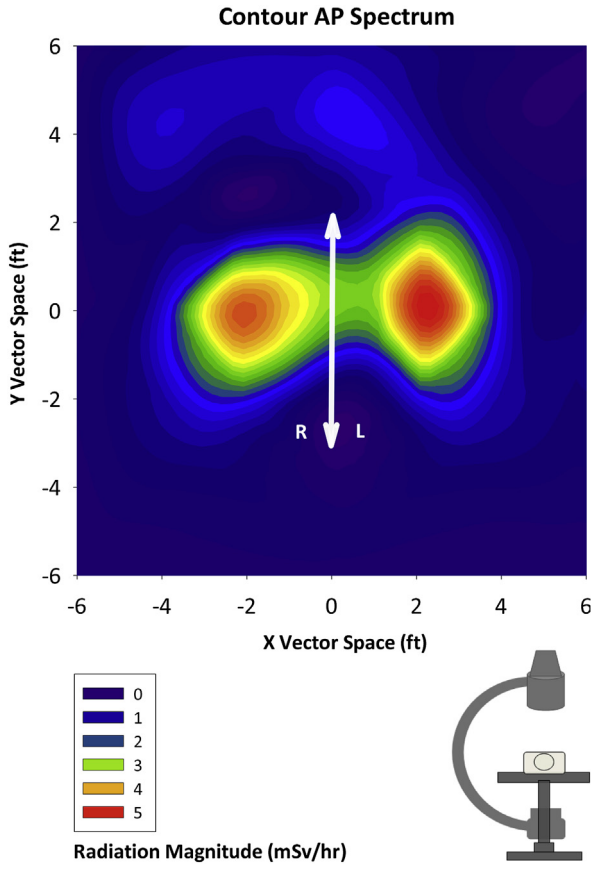

Fig 2. Contour anteroposterior (*AP*) plot for radiation dose levels surrounding the angiographic table (*arrow*). Coordinates along the X and Y vector spaces (0, 0) define the index image acquisition position. *L*, Left; *R*, right.

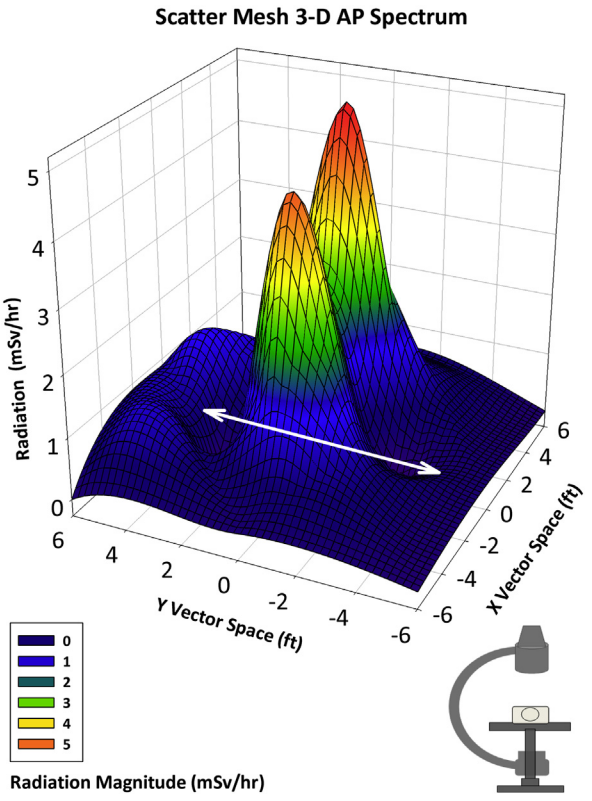

Fig 3. Scatter mesh three-dimensional (*3-D*) anteroposterior (*AP*) spectrum for radiation dose levels surrounding the angiographic table (*arrow*). Coordinates along the X and Y vector spaces (0, 0) define the index image acquisition position. A rational image of this graph is available in the Video accompanying this article (online only).

a single peak distribution pattern (Fig 4). Maximal exposure to radiation occurs on the emitter side of the angiographic table at the 2-ft distance perpendicular to the dose emitter (69 mSv/h; Fig 5). The radiation exposure along the ends of the head-foot axis is <0.77 mSv/h.

RAO 45° imaging. Digital subtraction RAO 45° imaging yields a single peak distribution pattern (Fig 6). Maximum exposure to radiation occurs on the emitter side of the angiographic table at the 2-ft distance perpendicular to the dose emitter (10.9 mSv/h; Fig 7). The radiation exposure along the ends of the head-foot axis is <0.77 mSv/h.

DISCUSSION

As a result of the increasing prevalence and complexity of catheter-based vascular procedures, vascular surgeons and interventionalists are potentially subject to an increasing occupational radiation exposure risk. Numerous studies have attempted to quantify the ill effects of occupational risks of radiation. Zielinski et al[14] published a study of a cohort of 67,562 medical workers in Canada from 1951 to 1987. Registry data for mortality, cancer incidence, and dosimetry data were obtained. Compared with the general population, these workers exposed to low-dose radiation over many years, had higher rates of thyroid cancer in men and women (odds ratio, 1.74), and had higher rates of primary liver cancer in women. The study also demonstrated an increase in the risk of all-cause mortality, all cancer, and cardiovascular disease with increasing radiation dose in this population.[14]

Scatter dynamics of DSA imaging in an interventional suite has not been modeled and characterized in any study to date. In this study, we used the non–formaldehyde-fixed cadaver of a recently deceased man as the closest possible model of a patient, because the repeated exposures required for this experiment would not be appropriate for a patient or volunteer. The cadaver had no implantable devices to impact scatter but did grossly seem to have normal bone density and water content. From these data, we constructed radiation scatter clouds that represented graphically the radiation level for each tested projection and at each location within the interventional suite.

In the AP view, a bimodal peak scatter cloud distribution was observed. The peak scatter cloud distribution is

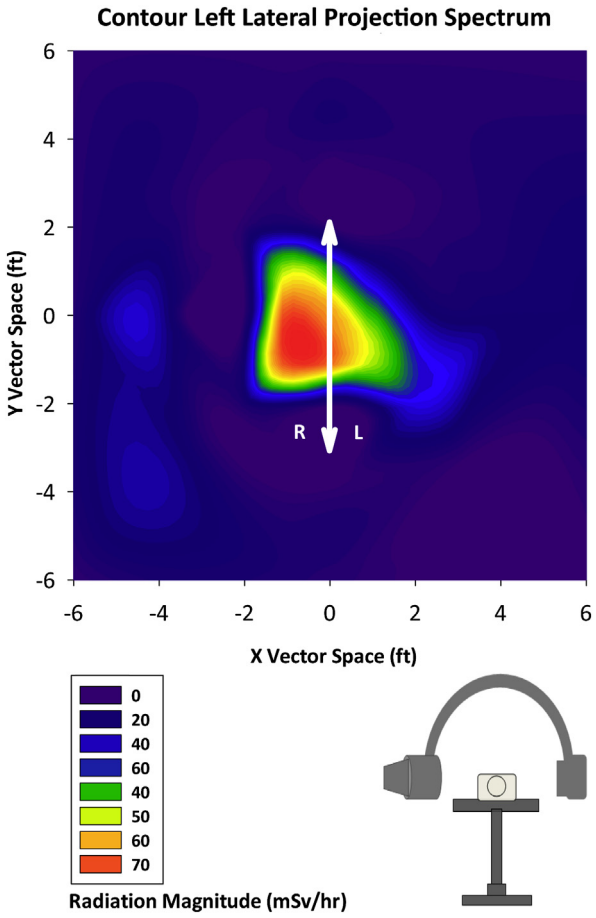

Fig 4. Contour left lateral plot shows radiation dose levels surrounding the angiographic table (*arrow*). Coordinates along X and Y vector spaces (0, 0) define the index image acquisition position. *L*, Left; *R*, right.

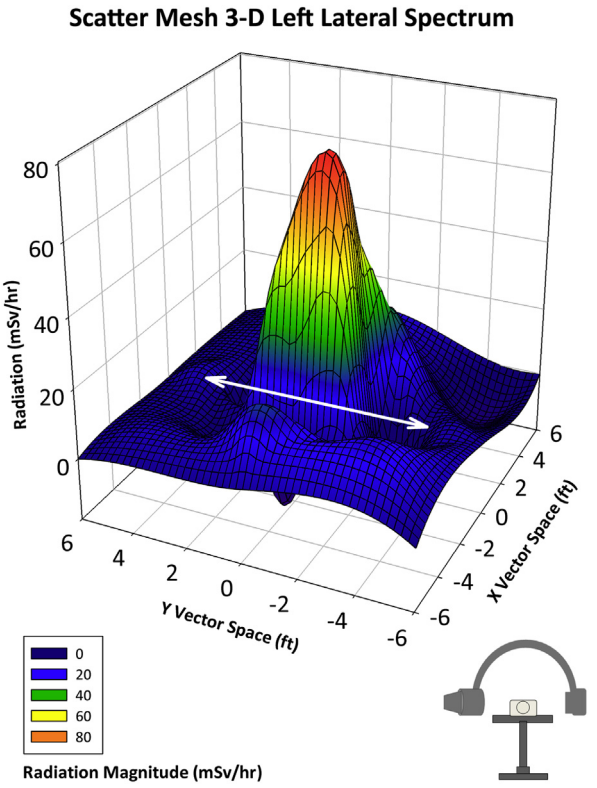

Fig 5. Scatter mesh three-dimensional (*3-D*) left lateral spectrum for radiation dose levels surrounding the angiographic table (*arrow*). Coordinates along the X and Y vector spaces (0, 0) define the index image acquisition position.

highest adjacent to the angiographic table at positions typical for the operator and assistant. Radiation patterns demonstrate minimal extensions along the head and foot axis of the angiographic table. Scatter radiation levels remain high within a 4-ft distance from the center of the imaged field. Plots of the radiation dose predicted by the inverse square law, compared with actual measured radiation scatter doses, demonstrate nonconformity (Fig 8). Radiation scatter doses in the AP view are higher than predicted, highlighting the complex effects of scatter.

The patient, or in our experiment, the cadaver, is the only object in the path of the primary x-ray beam; thus, it is evident that the patient is the initial source of scatter. Increasing body mass, bone density, and metallic implants are all thought to increase scatter. Although the scatter profiles of different patients may differ significantly, we believe that the use of a fresh human cadaver with repeated measurements of varying x-ray imaging techniques for this experiment provides the best possible approximation of an actual case. The design and materials used in the construction of the imaging equipment, table, and other variables also likely influence the radiation patterns observed.

Because suites are composed of varying arrays of walls and equipment, the simple inverse square law dynamics are not accurate. Increasing distance from the angiographic table decreases radiation exposure; however, the dose observed is higher than predicted according to point source calculations. Simply taking a step away from the angiographic table may not suffice to minimize the exposure risk.

In the full left lateral projection, a single unimodal peak was observed adjacent to the table on the side of the emitter. The exposure in this location is not only higher than other positions in the angiographic suite, but the absolute value of scatter radiation in the left lateral projection is also much greater than any other projection. The high peak distribution of radiation observed might be partly attributed to direct backscatter from the side of the patient that is close to the emitter, the DoseAware detector, and potentially, the uninformed operator. Principles of good radiation practice with positioning of the operator on the same side as the detector are affirmed by these data. Plotting the predicted radiation doses under the inverse square law compared with actual measured radiation in left lateral projections demonstrates nonconformity (Fig 9). Actual radiation scatter doses in the left lateral view

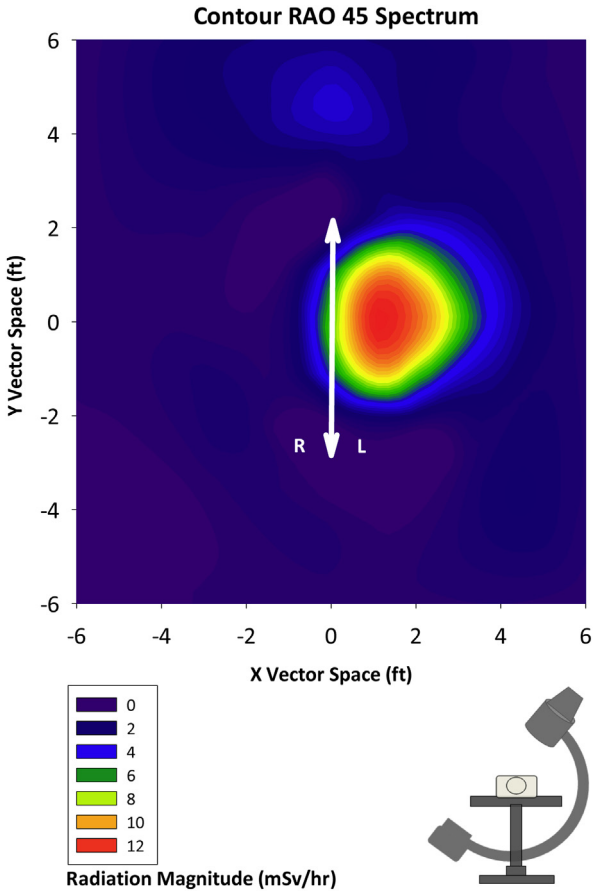

Fig 6. Contour right anterior oblique (*RAO*) 45° plot for radiation dose levels surrounding the angiographic table (*arrow*). The coordinates along the X and Y vector spaces (0, 0) define the index image acquisition position. *L*, Left; *R*, right.

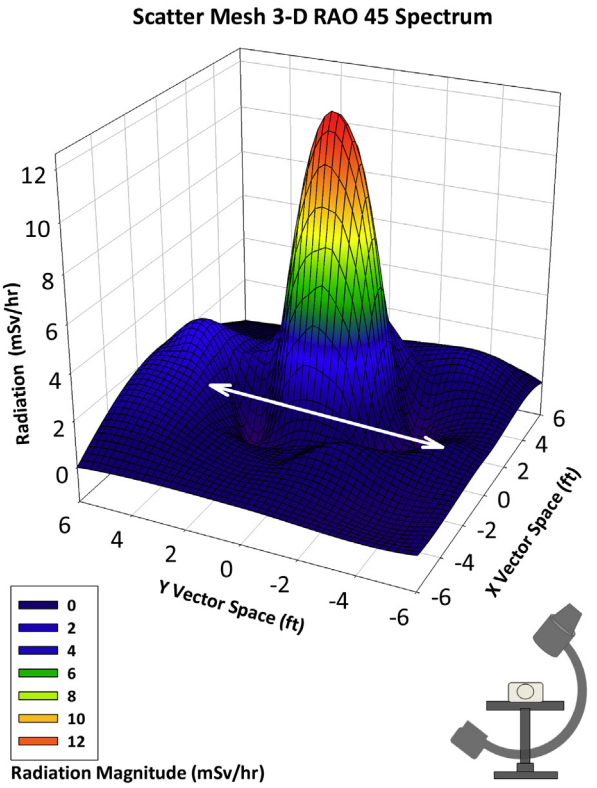

Fig 7. Scatter mesh three-dimensional (*3-D*) right anterior oblique (*RAO*) 45° spectrum for radiation dose levels surrounding the angiographic table (*arrow*). Coordinates along the X and Y vector spaces (0, 0) define the index image acquisition position.

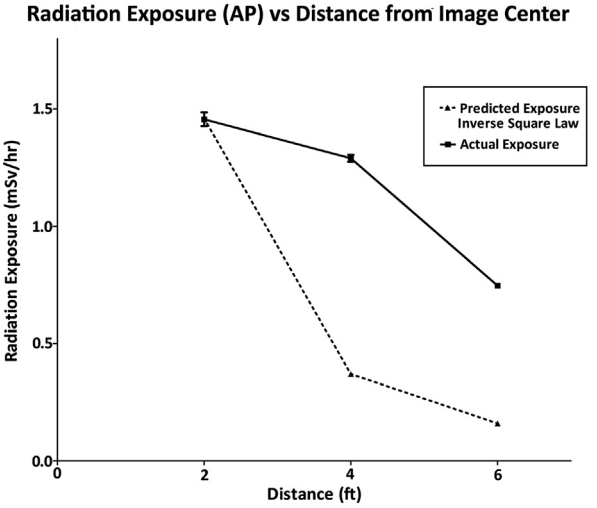

Fig 8. Scatter radiation at the 180° location (patient right, perpendicular to the table) imaging in the anteroposterior (*AP*) view with distance from image center for predicted inverse square law vs actual dose rates.

are higher than predicted, highlighting the complex effects of scatter.

In the RAO 45° projection, a single unimodal peak was observed adjacent to the table, again on the side of the emitter. Plotting the predicted radiation doses under the inverse square law with actual measured radiation in RAO projections demonstrates nonconformity; again, with actual radiation scatter doses observed being higher than predicted (Fig 10).

Although the laws of physics are uniformly applicable and the overall patterns of exposure presented here are likely generalizable, how closely the magnitude of the radiation exposure seen in this study will be reproduced in other angiography suites with different equipment and configurations remains to be seen. Because endovascular suite configurations vary significantly from site to site, scatter radiation patterns may not be predictable from a uniform equation. Each angiographic team may benefit by mapping the radiation levels produced in their particular facility and examining the imaging techniques used in their practice. With this site-specific and case-specific information, personnel might choose to alter technique or at least position staff to minimize exposure to scatter radiation. Although we strongly advocate the use of shielding and other radiation protection measures, these methods were

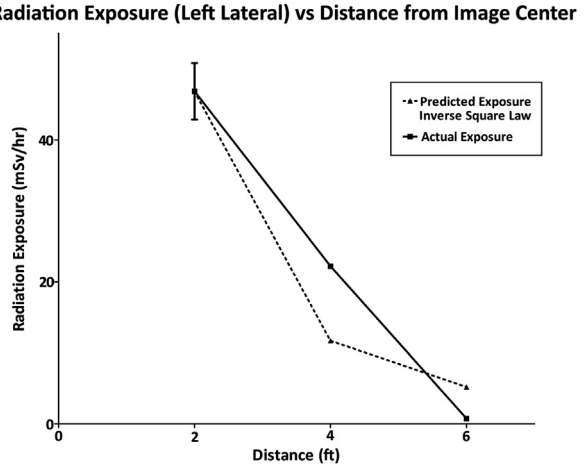

Fig 9. Scatter radiation at the 180° location (patient right, emitter side, perpendicular to the table) imaging in left lateral projection with distance from the image center for predicted inverse square law vs actual dose rates.

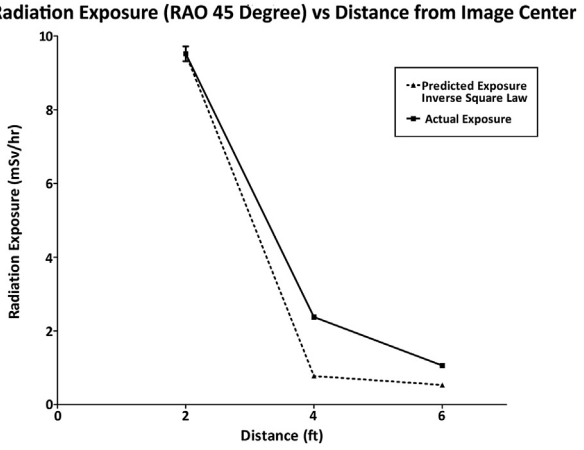

Fig 10. Scatter radiation at the 90° location (patient left, emitter side, perpendicular to the table) imaging in right anterior oblique (*RAO*) 45° projection with distance from image center for predicted inverse square law vs actual dose rates.

not used in this study, providing for unimpeded data for modeling.

Understanding the real risks of increased radiation exposure is integral to changing practice techniques. The mere theoretical understanding of radiation principles may not translate into uniform clinical practice. However, the data presented in this study provide a vivid representation of the uneven distribution of scatter radiation and the dramatic effect of changing imaging angles and one's position in the room. Visualization and characterization of scatter radiation is pivotal in guiding and establishing a new reality.

CONCLUSIONS

Exposure to scatter radiation is a real risk to the interventionalist and the endovascular team. This risk varies dramatically, depending on imaging technique and personnel position around the angiographic table. Unfortunately, the measured intensity of this scatter radiation did not drop off as the square of the distance from the source. The common practice during endovascular procedures of taking one step back from the table may not provide the level of safety that has traditionally been ascribed to it. The highest radiation doses were observed on the emitter side of the table, and therefore, special emphasis should be paid to moving staff away from the scatter source (ie, the patient) when standing on the emitter side of the table during high-dose DSA imaging. Demonstrating radiation scatter in the form of a scatter cloud plot allows easy visualization of the intensity of this radiation scatter effect, which differs markedly from what would be predicted from a simple application of the inverse square law. The ability to quantitate and express scatter dynamics through cloud constructs is a great addition to the armamentarium of the interventionalist seeking maneuvers and techniques to reduce the radiation risks to the team while providing optimal imaging for the patient.

AUTHOR CONTRIBUTIONS

Conception and design: OH, PA, MI
Analysis and interpretation: OH, PA, NH, MI
Data collection: OH, PA, MI
Writing the article: OH, PA, MI
Critical revision of the article: OH, PA, NH, MI
Final approval of the article: OH, NH, MI
Statistical analysis: OH, MI
Obtained funding: MI
Overall responsibility: OH

REFERENCES

1. Miller DL. Overview of contemporary interventional fluoroscopy procedures. Health Phys 2008;95:638-44.
2. Vano E, Gonzalez L, Fernandez JM, Haskal ZJ. Eye lens exposure to radiation in interventional suites: caution is warranted. Radiology 2008;248:945-53.
3. Stecker MS, Balter S, Towbin RB, Miller DL, Vañó E, Bartal G, et al. Guidelines for patient radiation dose management. J Vasc Interv Radiol 2009;20:S263-73.
4. Kim KP, Miller DL, Balter S, Kleinerman RA, Linet MS, Kwon D, et al. Occupational radiation doses to operators performing cardiac catheterization procedures. Health Phys 2008;94:211-27.
5. Klein LW, Miller DL, Balter S, Norbash A, Haines D, Fairobent L, et al. Occupational health hazards in the interventional laboratory: time for a safer environment. J Vasc Interv Radiol 2009;20: S278-83.
6. Marshall NW, Noble J, Faulkner K. Patient and staff dosimetry in neuroradiological procedures. Br J Radiol 1995;68:495-501.
7. BEIR V (Committee on the Biological Effects of Ionizing Radiation, Board on Radiation Effects Research, Committee on Life Sciences, National Research Council). Health effects of exposure to low levels of ionizing radiation. Washington, DC: The National Academies Press; 1990.
8. Roth J, Schweizer P, Guckel C. [Basis of radiation protection]. Schweiz Med Wochenschr 1996;126:1157-71.
9. Hayashi N, Sakai T, Kitagawa M, Inagaki R, Yamamoto T, Fukushima T, et al. Radiation exposure to interventional radiologists

during manual-injection digital subtraction angiography. Cardiovasc Intervent Radiol 1998;21:240-3.
10. Kuon E, Dahm JB, Empen K, Robinson DM, Reuter G, Wucherer M. Identification of less-irradiating tube angulations in invasive cardiology. J Am Coll Cardiol 2004;44:1420-8.
11. Kim KP, Miller DL. Minimising radiation exposure to physicians performing fluoroscopically guided cardiac catheterisation procedures: a review. Radiat Prot Dosimetry 2009;133:227-33.
12. Manchikanti L, Cash KA, Moss TL, Rivera J, Pampati V. Risk of whole body radiation exposure and protective measures in fluoroscopically guided interventional techniques: a prospective evaluation. BMC Anesthesiol 2003;3:2.
13. Mitchell EL, Furey P. Prevention of radiation injury from medical imaging. J Vasc Surg 2011;53:22-27S.
14. Zielinski JM, Shilnikova NS, Krewski D. Canadian National Dose Registry of Radiation Workers: overview of research from 1951 through 2007. Int J Occup Med Environ Health 2008;21:269-75.

Submitted Jan 21, 2012; accepted Jan 23, 2013.

Additional material for this article may be found online at www.jvascsurg.org.